Prediction of a mobile two-dimensional electron gas at the LaScO_{3}/BaSnO_{3}(001) interface

Tula R. Paudel and Evgeny Y. Tsymbal

Phys. Rev. B **96**, 245423 — Published 26 December 2017

DOI: 10.1103/PhysRevB.96.245423

Prediction of a Mobile Two-Dimensional Electron Gas at the $LaScO_3/BaSnO_3$ (001) Interface

Tula R. Paudel and Evgeny Y. Tsymbal

Department of Physics and Astronomy & Nebraska Center for Materials and Nanoscience, University of Nebraska, Lincoln, Nebraska 68588-0299, USA

Two-dimensional electron gases (2DEG) at oxide interfaces, such as $LaAlO_3/SrTiO_3$ (001), have aroused significant interest due to their high carrier density (~10^{14} cm^{-2}) and strong lateral confinement (~1 nm). However, these 2DEGs are normally hosted by the weakly dispersive and degenerate *d*-bands (e. g., Ti-3*d* bands), which are strongly coupled to the lattice, causing mobility of such 2DEGs to be relatively low at room temperature (~1 cm^2/Vs). Here, we propose using oxide host materials with the conduction bands formed from *s*-electrons to increase carrier mobility and soften its temperature dependence. Using first-principles density functional theory calculations, we investigate $LaScO_3/BaSnO_3$ (001) heterostructure and as a model system, where the conduction band hosts the *s*-like carriers. We find that the polar discontinuity at this interface leads to electronic reconstruction resulting in the formation of the 2DEG at this interface. The conduction electrons reside in the highly dispersive Sn-5*s* bands, which have a large band width and a low effective mass. The predicted 2DEG is expected to be highly mobile even at room temperature due to the reduced electron-phonon scattering via the inter-band scattering channel. A qualitatively similar behavior is predicted for a doped $BaSnO_3$, where a monolayer of BaO is replaced with LaO. We anticipate that the quantum phenomena associated with these 2DEGs to be more pronounced owing to the high mobility of the carriers.

I. Introduction

An interface between polar and non-polar complex oxides hosts a two-dimensional electron gas (2DEG), as well known when a polar $LaAlO_3$ (LAO) thin film is grown epitaxially along the [001] direction on a non-polar $SrTiO_3$ (STO) substrate. [1] Due to LAO consisting of the alternating $(LaO)^{+1}$ and $(MO_2)^{-1}$ charged planes, polar discontinuity at the interface creates an increasing electrostatic potential in the system. To eliminate the diverging potential, half an electron per unit cell area is transferred to the LaO/TiO_2-terminated LAO/STO (001) interface – the mechanism known as electronic reconstruction induced by polar catastrophe,[2] forming a 2DEG.

The 2DEG gas has high carrier density (~10^{14} cm^{-2}), strong lateral confinement (~1 nm), and relatively high mobility (~10^4 cm^2/Vs) at low temperature, which makes it attractive for various electronic and optoelectronic applications. The mobility, however, decreases quite dramatically as a function of temperature, and at room temperature its becomes ~1 cm^2/Vs.[1] This significant reduction is largely due to the nature of the orbitals involved in the electronic reconstruction. In the LAO/STO system, the conduction electrons are hosted by the Ti-3*d* orbitals of the t_{2g} symmetry forming the STO conduction bands. In bulk STO, these bands are relatively non-dispersive and have large effective mass, m^*, which on its own reduces the electron mobility, $\mu_e = e\tau/m^*$ (here e is electronic charge and τ^{-1} is the scattering rate). In addition, these bands are fully degenerate at the Brillouin zone center and partly degenerate along high symmetry directions. The carriers residing on these bands can therefore scatter by an impurity or a phonon via multiple scattering channels involving intra-band or inter-band transitions. The electron mobility is therefore reduced in comparison to a system with a single non-degenerate conduction band due to a higher scattering rate and have a stronger temperature dependence due to opening multiple scattering channels on thermally populated phonon modes.

In LAO/STO (001) heterostructure, the quantum confinement splits the t_{2g} symmetry band to a lower energy d_{xy} band and higher energy d_{xz} and d_{yz} bands[3]. At low temperature, the conduction is dominated by a dispersive non-degenerate d_{xy} band and hence the mobility is high. However, when temperature increases, heavier degenerate d_{yz} and d_{xz} bands get involved

in the conduction by providing states for scattering of the mobile d_{xy} electrons via electron-phonon-coupling and inter-band transitions. In addition, the electron-phonon coupling leads to the formation of polarons, which reduce the electron mobility when temperature increases.[4]

The low mobility and high carrier concentration at the LAO/STO interface makes it harder to study quantum phenomena expected for a 2DEG, such as the fractional and quantum Hall effects.[5] To realize such effects at a reasonable magnetic field, B ~ 10T, the condition for quantum conductance oscillations requires the cyclotron frequency, $\omega_c = eB/m^*$, to satisfy the condition, $\omega_c\tau = \mu_e B > 1$, [6] which in turn requires the mobility μ_e to be higher than 1000 cm^2/Vs. [7] A large effective mass reduces the energy separation (~ω_c) between the Landau levels and makes observing the quantized levels more difficult. Since m^* is determined by the materials choice, one can enhance the electron mobility by decreasing carrier density, e. g. using the electrostatic field effect,[8,9,10,11] surface adsorbates,[12] or interface engineering.[13] However, so far the quantum Hall effect has not been reported for the LAO/STO and related systems with the exception of the delta-doped STO.[5]

These fundamental problems associated with the *d*-orbital character of the conduction bands can be alleviated by choosing host materials with the conduction bands fully composed of highly dispersive non-degenerate *s*-orbitals. An *s*-band has a large band width, a low effective mass, and due to their non-degenerate character is expected to have fewer scattering channels – in fact, the inter-band scattering channel is entirely turned off. The lighter carriers with a longer life time give rise to higher mobility. As the result, one would expect a weaker temperature dependence compared to the system where the conduction is controlled by multiple *d*-bands. In addition, quantum phenomena associated with such a 2DEG electron gas are expected to be more pronounced and easier to observe.

As a model system for the host oxide materials with *s*-like conduction bands, we consider an interface between non-polar perovskite $BaSnO_3$ (BSO) and polar perovskite $LaScO_3$ (LSO) stacked along the [001] direction. Using first-principles density functional theory calculations, we find that the polar discontinuity induced carriers reside in the conduction band of $BaSnO_3$ formed from the Sn-5*s* orbitals. These bands have low effective mass and low density of states and hence are expected to have high mobility. The highly dispersive conduction bands form well separated quantized energy levels and step-like quasi two-dimensional density of states.

II. Computational Methods

We employ the projected augmented wave (PAW)[14] method for the electron-ion potential and the local density approximation (LDA) for exchange-correlation potential,[15] as implemented in Vienna *ab-initio* simulation package (VASP).[16] The pseudopotential includes non-linear core-correction[17] as described in ref. 15. The Ba pseudopotential includes the semi-core 5*s* states along with the valence $5p^6 6s^2$ states, while the pseudopotentials of other elements include only the valence states: $4s^1 3d^3$ for Ti, $4s^2 3d^1$ for Sc, $4s^2 4p^6 6s^2 5d^1$ for La, $5s^2 5p^2$ for Sn, and $2s^2 2p^4$ for O. The calculations are carried out using the kinetic energy cutoff of 340 eV and 6×6×1 *k*-point mesh for Brillouin zone integration. We fully relax ionic coordinates with the force convergence limit of 0.001 eV/atom.

III. Results and Discussion

A. Bulk $BaSnO_3$ and $LaScO_3$

Perovskite BSO and LSO single crystals are both large band gap semiconductors with experimental lattice constants of 4.05 Å[18] and 4.12Å [19]and band gaps of ~3 eV [20,21,22,23] and 5.7eV[24], respectively. The Goldsmith tolerance factor is ~0.92 for BSO and supports its pseudocubic structure, whereas that is much lower, i.e. ~0.8, for LSO and produces octahedral distortions resulting in the orthorhombic structure.[25] Fig. 1a shows the cubic unit cell of BSO, and Fig. 1b shows the orthorhombic unit cell of LSO where $GdFeO_3$-type distortions have $a^-b^+a^-$ distortion pattern in the Glazer notation. On their own, epitaxial LSO films[26] have been investigated as high-*k* dielectrics,[27] while BSO has been considered as high mobility transparent conducting oxide.[28,29,30,31] At room temperature doped BSO films reveal mobility of $\sim 320\ cm^2/Vs$ [28] compared to ~10 cm^2/Vs for doped STO.[32] This relatively high mobility of BSO originates from the highly dispersive conduction bands, which are formed from the non-degenerate Sn-5*s* orbitals (Fig. 1a). This is very different from STO, where the conduction bands are formed of the non-dispersive Ti-3*d* orbitals degenerate at the Γ point (Fig. 1c). The low effective mass (~0.3 m_0, where m_0 is a free electron mass) and a non-degenerate character of the *s*-orbitals support the high carrier mobility in BSO up to room temperature.

In our calculations, the pseudocubic lattice constants of bulk BSO and LSO are found to be 4.10 and 3.99 slightly smaller than the experimental counterparts 4.05 [18] and 4.12 [19] respectively. The calculated band gaps of bulk BSO and LSO are found to be 0.96 eV and 2.7 eV, which are again lower than the respective experimental values of ~3 eV [20, 21, 22, 23] and 5.7eV [24] respectively. This underestimation of lattice constants and band gaps is well known deficiency of the local density approximation. We find that in both compounds the valence band maxima are formed from the oxygen *p*-orbitals. The conduction band minimum is dominated by the Sn-5*s* orbitals in BSO and by the Sc-3*d* orbitals in LSO.

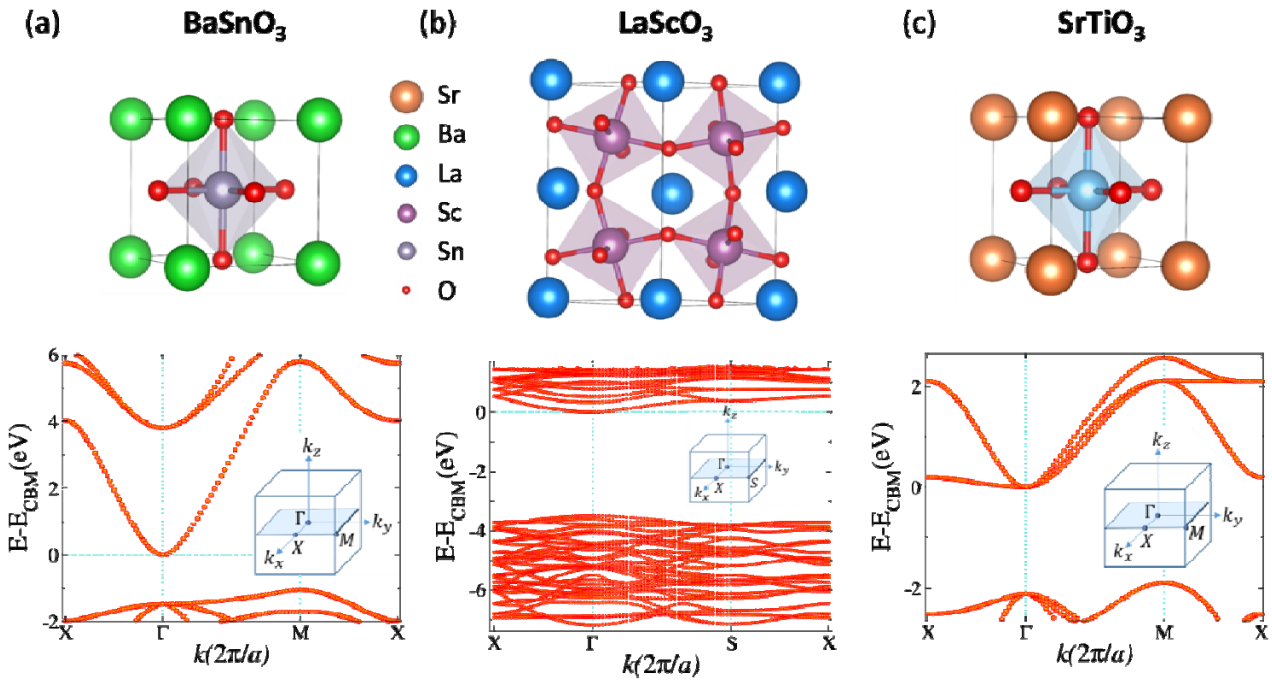

Figure 1: Calculated atomic (top panels) and electronic (bottom panels) structures of bulk cubic $BaSnO_3$ (a), orthorhombic $LaScO_3$ (b), and cubic $SrTiO_3$ (c). Insets in the bottom panels show the Brillouin zones of the compounds.

B. $BaSnO_3/LaScO_3$ (001) Heterostructure

We explore the electronic properties of the LSO/BSO (001) interface using theoretical calculations based on density functional theory (DFT). The LSO/BSO (001) interface is modelled using a $(LSO)_m/(BSO)_n$ slab (Fig. 2a) with $n = 5$ unit cells (u.c.) and $m = 1, 2, \ldots 6$ u.c.

separated by a 16Å vacuum layer. In the calculations, we assume the in-plane theoretical lattice constant of BSO, a = 4.10 Å, which leads to the top LSO layer being under tensile bi-axial strain of about 2.7%. A dipole layer is introduced in the vacuum region of the supercell to eliminate a non-physical electric field emerging in vacuum due to the periodic boundary conditions. [33] The dielectric constants of BSO and LSO are calculated using density functional perturbation theory[34,35] as implemented in VASP. We find that the dielectric constant $\varepsilon_r = 68$ for BSO and $\varepsilon_r = 29$ for LSO, both being dominated by the ionic contribution with values of about 62 and 24, respectively. The calculated value of the dielectric constant of LSO is in line with the known experimental values of 22 for LSO films grown in SiO_2[36] and 32 for LSO films grown on LAO.[18]

In the charge neutral BSO, Sn is nominally in 4+ oxidation state, Ba is in 2+ oxidation state, and O is in 2– oxidation state, so that along the [001] direction both SnO_2 and BaO layers are charge neutral. However, in LSO, La and Sc are in 3+ oxidation state, while O is in 2– oxidation state, so that along the [001] direction LaO layers are is positively charged, while ScO_2 layers are negatively charged. In bulk, these ionic charges cancel each other so that the system remains neutral. However, in the slab geometry, where the bottom layer of LSO is terminated with positively charges $(LaO)^{+1}$ while the top layer is terminated with negatively charged $(ScO_2)^{-1}$, the charge compensation is incomplete resulting in a surface polarization charge. This polarization charge has positive surface charge density of $\sigma_0 = +e/2a^2$ on the bottom surface of the slab and the negative surface charge density of $-\sigma_0 = -e/2a^2$ on the top surface of the slab. When such a LSO slab is stacked on top of the SnO_2-terminated BSO layer, as shown in Fig. 2a, the polarization charges induce an electric field of $E_0 = \sigma_0/\varepsilon_{LSO}$ (where $\varepsilon_{LSO} = \varepsilon_r\varepsilon_0$ is the dielectric permittivity of LSO) pointing from the interface to the surface of LSO, resulting in the increasing electrostatic potential when the LSO thickness increases. To eliminate (reduce) an energetically unfavorable electric field an electron charge is deposited onto the LSO/BSO interface, which is known as electronic reconstruction.

Electronic reconstruction leads to thickness dependent electron accumulation at the interface. The electric field in LSO leads to the potential buildup, $\Delta V = E_0 t$ (where t is LSO layer thickness) which shifts its bands up. This is seen from the calculated density of states (DOS) in Fig. 2b, where the LSO-projected DOS shifts rigidly up when moving from the LSO/BSO interface to the LSO surface. At a critical thickness t_c, the LSO valence band shift

becomes equal to the band gap of BSO (, i.e. , so that at larger LSO thickness electrons start to transfer from the top of the LSO valence band to the bottom of the BSO conduction band. Using the calculated band gap BSO of 0.96 eV and the calculated dielectric constant of LSO of = 29 we find, according to this model, that the LSO critical thickness is 2 u. c. Our DFT calculation predicts however that the charge transfer to the LSO/BSO interfaces occurs when LSO has 3 u. c. thickness. Some disagreement between the polar catastrophe model and the explicit calculation likely comes from the LSO surface, which produces a stronger dielectric response to the electric field not taken into account within the simple model. Fig 2c shows BSO-projected DOS in the LSO/BSO heterostructure for different LSO thickness as a function of energy. It is seen that when LAO thickness is more than 3 u.c., the Fermi level (the zero energy) cuts through the bottom of the conduction bands, indicating that the LSO/BSO interface is *n*-type, while for smaller LSO thickness it lies below the conduction band minimum so that the interface is insulating.

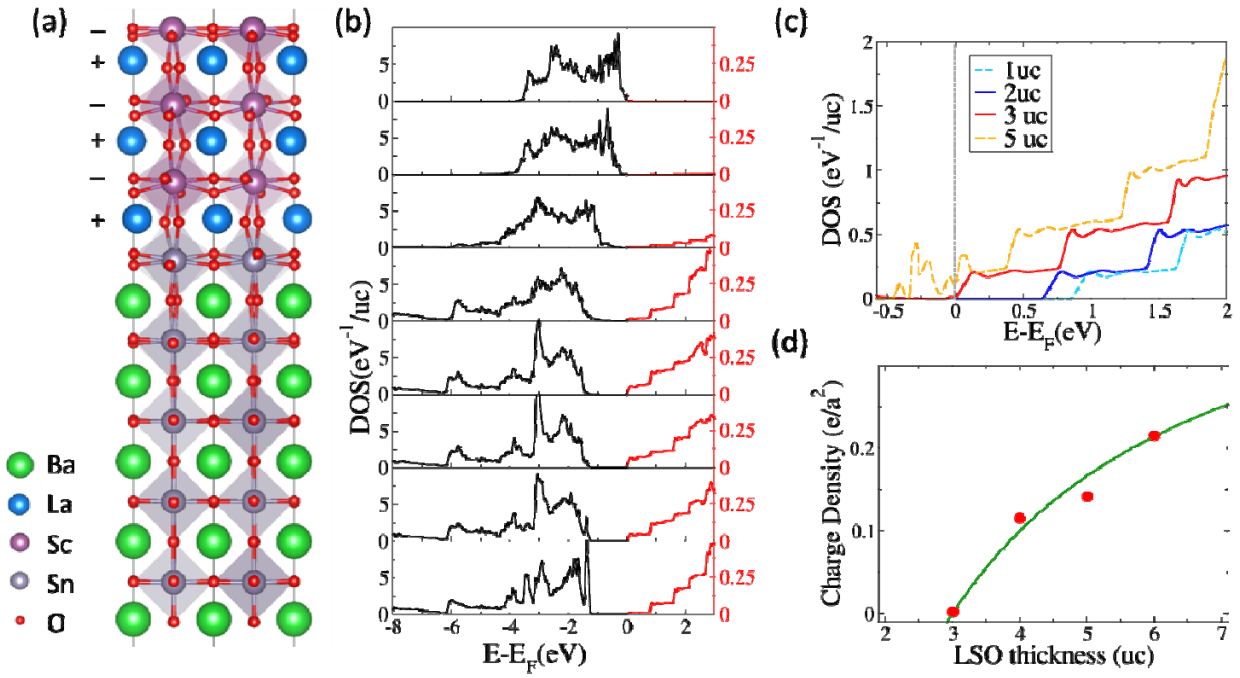

Figure 2: Atomic structure (a), layer-dependent (b) and BSO-projected (c) density of states (DOS) as a function of energy for $(LSO)_3/(BSO)_5$ heterostructure. The vertical lines in (b) and (c) indicate the Fermi energy. In (b) *y*-coordinate scale at left and right are different to reflect very different magnitude of DOS for the valence (black lines) and conduction (red lines) bands.

(d) – charge density σ as a function of LSO layer thickness m (given in unit cells) in a $(LSO)_m/(BSO)_5$ heterostructure. Points are the result of the DFT calculation, whereas the solid line is prediction of the model.

With increasing LSO thickness t, the electron charge $\sigma(t)$ transferred to the LSO/BSO interface reduces the electric field in LSO so that $E(t) = [\sigma_0 - \sigma(t)]/\varepsilon_{LSO}$. The corresponding potential drop is bounded by the band gap of BSO, which implies that $E(t)t = E_0 t_c$, resulting in $\sigma(t) = \sigma_0(1 - t_c/t)$. This result is well known for the LAO/STO case.[37] In Fig. 2d we plot the transferred charge per area of the psedocubic unit cell, which is calculated explicitly by integrating the DOS of the BSO conduction band up to Fermi level (dots in Fig. 2d), and compare it to the prediction of this simple model (the solid line in Fig. 2d) where t_c was assumed to be 3 u.c. As seen from the plot, the calculated carrier density is roughly consistent with that predicted using this simple model.

The electric field in LSO induces polarization pointing to the surface. The off-center displacement directly captures magnitude and direction of the polarization. Fig. 3a shows the off-center displacement in the BSO and LSO layers. Here, we define the off-center displacement as the difference between the longer and shorter bonds, b_l and b_s along the z-direction in B-centered (Sn in BSO and Sc in LSO) octahedral cage as shown in inset of Fig. 4a. Due to the electric field pointing away from the interface, the B-site cation moves towards the surface resulting the Sc-O bonds to be shorter toward the surface and longer toward the interface. The difference between these bonds is positive and large in LSO indicating that the LSO polarization is pointing from the interface to the surface. As expected, the off-center displacement in BSO drops down quickly as a function of distance from the interface, as there is no field to push ions. Similar to B cations, A cations (La in LSO and Ba in BSO) are also pushed away from the interface by the polar field. As a result, the A-O displacement along the z-direction is positive in LSO and negative nearby the interface in BSO as shown in Fig 2b. The later displacement drops down in BSO similar to the off-center displacement as there is no field to sustain it in a long range. These structural changes are similar to those known for the LAO/STO interface.[38]

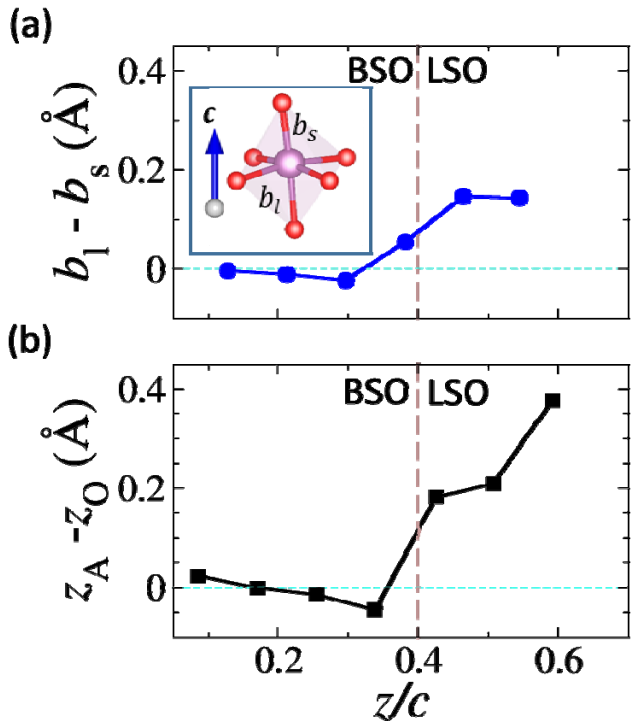

Figure 3: Structural distortions in the $(LSO)_3/(BSO)_5$ heterostructure as a function of reduced coordinate (z/c): (a) B-cation displacement with respect to center in oxygen octahedral cage, (b) A- cation displacement with respect to the oxygen in the plane. The off-center B-cation displacement is defined as difference in bond lengths shown in inset. Positive displacement in LSO and negative displacement in BSO imply movement of cations away from the interface.

Despite similarity of the mechanisms behind appearance of 2DEG and structural changes associated with the polar interfaces in the LSO/BSO and LAO/STO systems, the character of the 2DEG at the LSO/BSO interface is quite different. Fig. 4a shows the band structure of the LSO/BSO heterostructure with 3 unit cells of LSO. As can be seen from the figure, the conduction bands are very dispersive and formed from the Sn-5*s* orbitals at the center of the Brillouin zone. In table I, we tabulate the effective mass of the lowest five quantized bands along the high symmetry and directions in the orthorhombic Brillouin zone. From the table it can be seen that the effective mass is , i. e. it is similar to that observed for bulk BSO. This value is in a qualitative agreement with the effective mass of ~0.2 calculated

using a hybrid functional.[39] There is some anisotropy in the effective mass: it is lower along the direction as compared to the direction. Additionally, the bands become progressively heavier at higher energy due to stronger hybridization with the O-p_z orbitals. Fig. 4b shows the DOS of the occupied Sn-5*s* bands as a function of energy. The density of states increases in a stepwise fashion at each quantized level revealing a possibility of quantized conductance as a function of voltage.

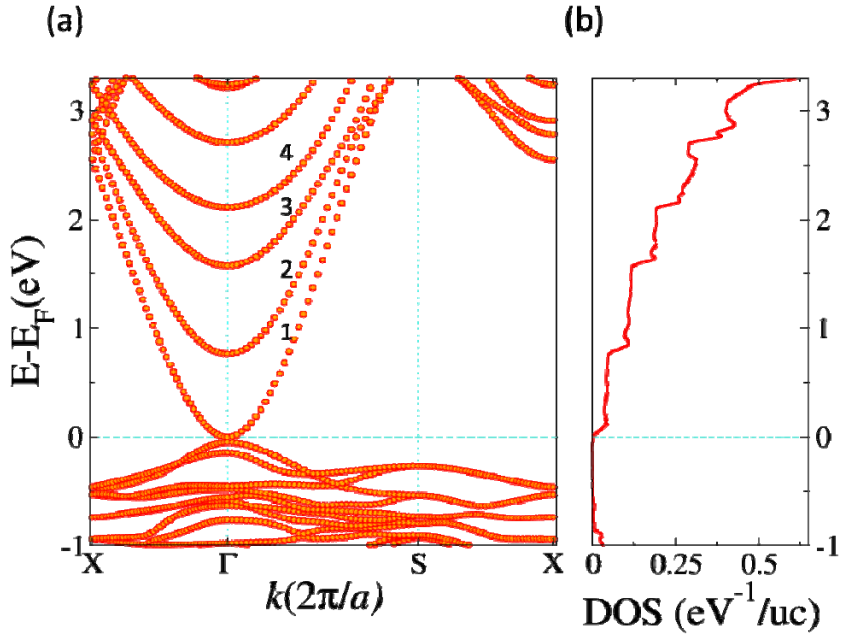

Figure 4: Band structure of the $(LSO)_3/(BSO)_5$ heterostructure (a) and density of states (DOS) projected to the BSO (b). In (b) only the conduction band DOS is shown. The dotted horizontal line represents the Fermi energy.

This behavior is different from what is known for the LAO/STO (001) interface, where 2DEG is hosted by rather localized Ti-3*d* bands. Due to the quantum confinement the T_{2g} bands split into the bands and bands. The bands are relatively dispersive and have a low effective mass (~0.4 [40]) at the zone center. They lie at a lower energy and thus are occupied first.[41] With increasing the carrier concentration above critical density *e*/cm^2 the carriers start to occupy the bands, which are less dispersive and have much higher effective mass (up to [11,42]) affecting the overall mobility. Hybridization between the bands of different symmetry as well as open channels for inter-band transitions leads to

stronger scattering and low mobility. The latter contribution contributes significantly to the mobility drop with increasing temperature due to population of phonon modes with higher energy and electron-phonon scattering. The room temperature mobility of 2DEG at the LAO/STO interface is dismal ~1 cm^2/Vs despite its promising value of >10,000 cm^2/Vs at low temperature. [1,2]

Table 1: Effective mass of the conduction bands in the LSO (3 u.c.)/BSO (5 u.c.) heterostructure and delta-doped BSO along the $\Gamma - X$ and $\Gamma - S$ lines in the Brillouin zone. The bands are numbered starting from bottom of the conduction band as indicated in Figs. 4a and 5c.

Band	**Heterostructure**		**Delta-Doped**	
	$\Gamma - X$	$\Gamma - S$	$\Gamma - X$	$\Gamma - M$
1	0.35	0.33	0.31	0.32
2	0.47	0.44	0.34	0.36
3	0.68	0.64	0.31	0.33
4	0.93	0.89	0.44	0.48
Bulk	0.29	0.30	0.29	0.30

The electron mobility at the LSO/BSO interface is expected to be higher for two reasons. First, the effective mass of the 2DEG at the LSO/BSO (001) interface ($\sim 0.3\, m_0$) is lower than the effective mass of the lightest d_{xy} electrons at LAO/STO (001) interface ($\sim 0.4\, m_0$). Second, in the low carrier density limit, the conduction happens through a single non-degenerate Sn-5*s* band and there is no scattering channel for carriers via inter-band transitions. At higher carrier density, several quantized level are populated, but they have similar velocity and the effective mass. The quantized bands a well separated in energy not allowing for the inter-band transitions to occur driven by impurity scattering. The wide Sn-5*s* conduction band can accommodate the maximum possible 2DEG density of 0.5 e/a^2, which is not possible in the for the d_{xy} band in the LAO/STO system. The 2D free-electron model predicts the energy increase of $\Delta E = \hbar^2 \pi n/m \sim 2.4$ eV when depositing $n = 0.5\ e/a^2$ in BSO, while the *s*-state is ~ 4 eV wide. In fact, the value is ΔE is

expected to be even lower due to the presence of multiple quantum states, as will be seen from the results discussed below for the delta-delta doped BSO.

Furthermore, the temperature dependence of the carrier mobility in the LSO/BSO system is expected to be softer than that in the LAO/STO case. The temperature dependence of mobility $\mu = ne\tau/m^*$ is largely determined by the temperature dependence of the relaxation time τ. The latter is controlled by electron-phonon coupling, which produces scattering between different electronic states through intra-band and inter-band transitions and involves an electron-phonon coupling matrix and phonon-mode population.[43] The former is largely temperature independent, whereas the latter changes with temperature. In the LAO/STO system, where the electronic density of states is large, there are many channels open for scattering due to the *d*-bands being flat and nearly degenerate. With increasing temperature, more phonon modes are populated allowing for transitions between these electronic states. On the contrary, in the LSO/BSO where the *s*-bands control the conduction, the electronic density of states is small due to the dispersive nature of the *s*-bands. The inter-band scattering is therefore reduced as there are no many electronic states available in the energy range of phonon spectrum. The inter-band transition channel for electron-phonon scattering is fully suppressed due to the quantized bands being well-separated in energy. Thus, it is expected that reduction in mobility with increasing temperature will be much weaker for the LSO/BSO interface as compared to the LAO/STO interface. In fact, the doped bulk BSO is reported to have room temperature mobility of about μ = 320 cm^2/Vs [28] and conductivity $\sigma \sim 10^4$ S/cm [44] compared to $\mu \sim 10$ cm^2/Vs and $\sigma \sim 10$ S/cm for doped STO.[45,46]

C. Delta Doped $BaSnO_3$

Another way of attaining a 2DEG is delta-doping when a neutral ionic AO monolayer in an ABO_3 perovskite is replaced with $(A'O)^{+1}$.[47,48] Such an approach can be applied to BSO by substituting a BaO monolayer with a $(LaO)^{1+}$ monolayer, as shown in Fig 5a. The $(LaO)^{1+}$ monolayer serves a donor providing one electron per lateral unit cell area a^2 which is accumulated in BSO equally on either side of LaO. Comparing to the LSO/BSO case, the delta-doped system can be thought as an overlap of two interfaces with the interfacial charge density of 0.5 e/a^2, which is approached at the LSO/BSO interface when the top LSO layer thickness becomes large.

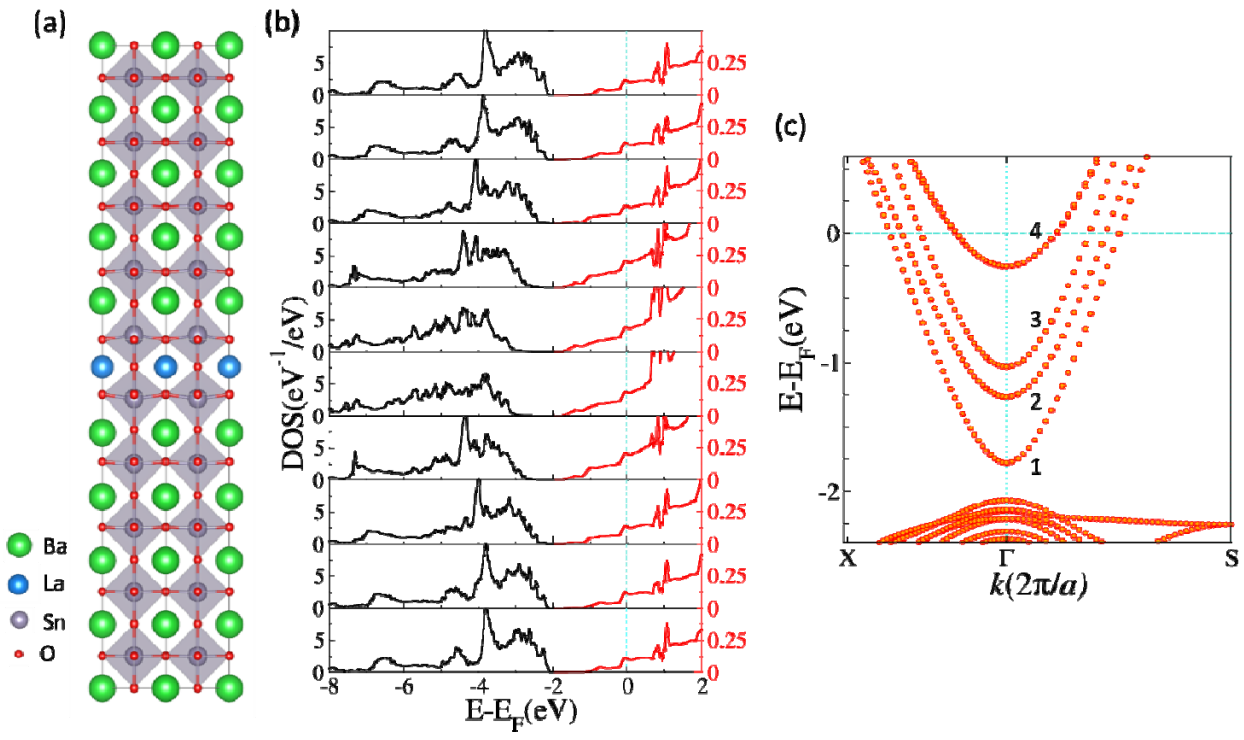

Figure 5: Atomic structure (a) and layer-dependent density of states (DOS) as a function of energy (b) and band structure (c) of a delta doped BSO with LaO layer at the middle. The vertical line indicates the Fermi energy. In (b) the y-coordinate scale at left and right are different to reflect very different magnitudes of DOS for the valence (black lines) and conduction (red lines) bands.

The atomic and electronic structure calculations of the delta-doped BSO are performed using a 10 u.c. BSO where the middle BaO layer is replaced with LaO (Fig. 5a). Fig 5b shows the calculated layer resolved DOS. Overall, it looks similar to the layer resolved DOS at the LSO/BSO interface (Fig 1b). However, in the case of the delta-doped BSO, the Fermi level lies much deeper in the conduction band of the BSO due to higher electron density. The band structure of the delta-doped BSO shown in Fig. 5c also resembles the band structure of the LSO/BSO heterostructure (Fig. 4a). There are several quantized states, four of them being partly filled in the delta-doped case. These bands are made of Sn-5*s* orbitals, are highly dispersive, and have low effective mass as shown in Table I.

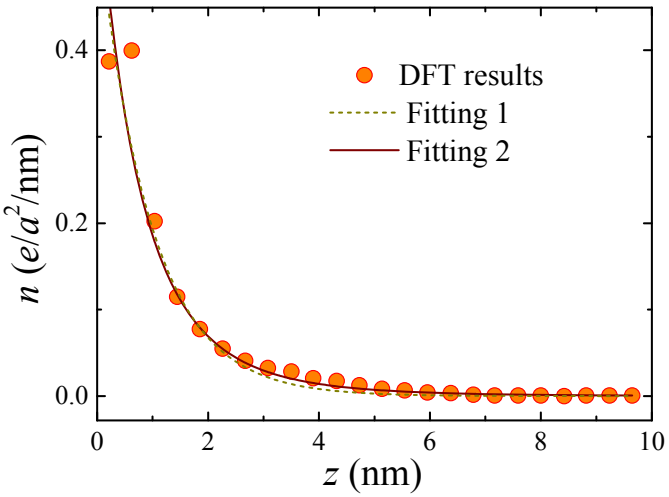

Figure 6: Charge density n as a function of z in a 51 u.c. BSO with a LaO monolayer replacing BaO in the middle of the supercell. LaO monolayer is positioned at z = 0. Results of the DFT calculation (dots) are fitted with $n(z) = \sigma_0 \exp(-z/\lambda)/\lambda$ (Fitting 1, dashed line) and $n(z) = 5\delta^5\sigma_0/(x+\delta)^6$ (Fitting 2, solid line), for $\sigma_0 = 0.5e/a^2$, resulting in $\lambda = 0.96$ nm and $\delta = 4.8$ nm.

D. 2DEG Confinement Width

In order to explore the scale over which the 2DEG is confined, we performed an additional calculation using a large 1x1x51 supercell of BSO with a LaO monolayer replacing BaO in the middle of the supercell. Figure 6 shows the calculated charge density as a function of distance from the LaO layer positioned at z = 0. Here each point in the plot was obtained by integrating the local DOS in a unit cell of BSO located at a certain distance from LaO. Due to mirror symmetry of the structure with respect to the LaO layer, the distribution is symmetric with respect to the z = 0 plane so that it has the same shape for negative z (not shown). It is evident from Fig. 6 that the charge density has a peak centered at z = 0 and the 2DEG is confined within a region of about 3 nm around LaO (where about 70% of carriers is located). A tail of the distribution extends somewhat up to 6 nm from the origin.

This behavior can be qualitatively understood within the Thomas-Fermi model (see, e.g., ref. 49), according to which the local chemical potential $\mu(z)$ is determined by the local charge

density $n(z)$ and related to the electrostatic potential $\varphi(z)$ as follows: $-e\varphi + \mu = E_F$, where E_F is the Fermi energy (which we assume to be zero). μ and n are linked through $n = \int_{-\infty}^{\mu} \rho(E)dE$, where $\rho(E)$ is the density of electronic states. The above equations couple $\varphi(z)$ and $n(z)$ which allows solving the Poisson equation $d^2\varphi/dz^2 = en/\varepsilon$, where ε in the dielectric permittivity of BSO. If the electron density is low, then only the lowest 2D sub-band is populated (band 1 in Fig. 5c) and in a free electron approximation the areal DOS ρ_{2D} is independent of energy E, i.e. $\rho_{2D} = m/(\pi\hbar^2)$, where *m* is an effective mass. The volume charge density can be estimated as $\rho = \rho_{2D}/a$, where *a* is the lattice constant of BSO. In this case, $n = \rho\mu = e\rho\varphi$, and solution of the Poisson equation is straightforward, resulting in $n(z) = n_0 \exp(-z/\lambda)$, where $\lambda = \sqrt{\varepsilon/(e^2\rho)}$. n_0 is determined from charge neutrality condition $\sigma_0 = e\int_0^{\infty} n(z)dz$, where σ_0 is the surface charge density (in our case 0.5 e/a^2). Within this model, we obtain $\lambda = \sqrt{a_0 a\varepsilon_r/m_r}/2$, where a_0 is the Bohr radius, ε_r is the relative dielectric constant of BSO, and $m_r = m/m_0$ is the reduced effective mass. Using $\varepsilon_r = 68$, $m_r = 0.35$, and $a = 4.1$ Å, we find $\lambda \approx 1.0$ nm. This estimate is surprisingly close to the value of λ we find by fitting the DFT results with the exponential function $\sigma_0 \exp(-z/\lambda)/\lambda$ (normalized to provide the total surface charge density $\sigma_0 = 0.5e/a^2$). The best fit is obtained for $\lambda \approx 0.96$ nm and shown in Fig. 6 by the dashed line.

In reality, however, when $\sigma_0 = 0.5e/a^2$, it is not just the lowest energy sub-band which is populated, but there are 4 bands crossing the Fermi energy (Fig. 5c). In this case, $\rho(E)$ is a step function of energy (like that shown in Fig. 4b). In this case, solution of the Poisson equation can be represented in terms of the piecewise exponential functions having different decay constants λ in different ranges of $\varphi(z)$ and hence $n(z)$. In the limit of large electron density (when many sub-bands are populated), we can assume that the charge density is given by a 3D free-electron model, $n = (2m/\hbar^2)^{3/2}\mu^{3/2}/(3\pi^2)$, resulting in the Poisson equation $d^2\varphi/dz^2 = e^{5/2}(2m/\hbar^2)^{3/2}\varphi^{3/2}/(3\pi^2\varepsilon)$. Solution of this equation is given by $\varphi(z) = A(e/\varepsilon)/(z+\delta)^4$, where $A = (225\pi/32)(a_0\varepsilon_r/m_r)^3$. This leads to the charge density

$n(z) = 20A/(z+\delta)^6$, where charge neutrality requires $\delta = (4Ae/\sigma_0)^{1/5}$. Using the known constants appropriate for BSO, we find within this approximation that $\delta \approx 7.8$ nm. This value is somewhat larger than that we obtain by fitting the DFT results with the $n(z) = 5\delta^5(\sigma_0/e)/(x+\delta)^6$ function (normalized to provide the total surface charge density $\sigma_0 = 0.5e/a^2$), where δ is treated as a fitting parameter. The best fit is obtained for $\delta \approx 4.8$ nm and shown in Fig. 6 by the solid line. It is evident from Fig. 6 that both approximations provide a similar and qualitatively reasonable trend describing the charge density as a function of *z*.

IV. Conclusions

We predict the presence of a two-dimensional electron gas at the polar LaO/SnO_2-terminated $LaScO_3/BaSnO_3$ (001) interface. The 2DEG is derived from the Sn-5*s* bands, which are highly dispersive and have effective mass of about 0.3 m_0. Contrary to the well-known $LaAlO_3/SrTiO_3$ (001) system, the predicted 2DEG is expected to reveal high mobility at room temperature. The *s*-character of the conduction bands and their low effective mass allow for accommodation of the largest possible carrier density of 0.5 electrons per lateral unit cell area without populating orbitals of other character. This property is demonstrated using a relevant example of the 2DEG at the delta-delta doped $BaSnO_3$, where a BaO monolayer is replaced with LaO. We find that the confinement width is about 3 nm and that the electron confinement can be reasonably well described with the Thomas-Fermi model. The electron confinement produces a number of non-degenerate quantized electronic states well separated in energy. This feature may be interesting for observing a quantized conductance in this system. We encourage the experimentalists working in the field of oxide heterostructures to explore the proposed systems.

Acknowledgements

This work was supported by the National Science Foundation (NSF) under the DMREF Grant No. DMR-1629270. Computations were performed utilizing the Holland Computing Center at the University of Nebraska.

[1] A. Ohtomo and H. Y. Hwang, Nature **427**, 423 (2004).

[2] N. Nakagawa, H. Y. Hwang, and D. A. Muller, Nat. Mater. **5**, 204 (2006).

[3] Z. S. Popović, S. Satpathy, and R. M. Martin, Phys. Rev. Lett. **101**, 256801 (2008).

[4] C. Cancellieri, A. S. Mishchenko, U. Aschauer, A. Filippetti, C. Faber, O. S. Barišić, V. A. Rogalev, T. Schmitt, N. Nagaosa, and V. N. Strocov, Nat. Comm. **7**, 10386 (2016).

[5] Y. Matsubara, K. S. Takahashi, M. S. Bahramy, Y. Kozuka, D. Maryenko, J. Falson, A. Tsukazaki, Y. Tokura, and M. Kawasaki, Nat. Comm. **7**, 11631 (2016).

[6] T. Ando, A. Fowler, and F. Stern, Rev. Mod. Phys. **54**, 438 (1982).

[7] A. D. Caviglia, S. Gariglio, C. Cancellieri, B. Sacépé, A. Fête, N. Reyren, M. Gabay, A. F. Morpurgo, and J.-M. Triscone, Phys. Rev. Lett. **105**, 236802 (2010).

[8] A. D. Caviglia, S. Gariglio, N. Reyren, D. Jaccard, T. Schneider, M. Gabay, S. Thiel, G. Hammerl, J. Mannhart, and J.-M. Triscone, Nature **456**, 624 (2008).

[9] K. Ueno, S. Nakamura, H. Shimotani, A. Ohtomo, N. Kimura, T. Nojima, H. Aoki, Y. Iwasa, and M. Kawasaki, Nat. Mater. **7**, 855 (2008).

[10] C. Bell, S. Harashima, Y. Kozuka, M. Kim, B. G. Kim, Y. Hikita, and H. Y. Hwang, Phys. Rev. Lett. **103**, 226802 (2009).

[11] A. P. Petrović, A. Paré, T. R. Paudel, K. Lee, S. Holmes, C. H. W. Barnes, A. David, T. Wu, E. Y. Tsymbal, and C. Panagopoulos, Sci. Reports **4**, 5338 (2014); New J. Phys. **16**, 103012 (2015).

[12] Y. Xie, C. Bell, Y. Hikita, S. Harashima, and H. Y. Hwang, Adv. Mater. **25**, 4735 (2013).

[13] Y. Z. Chen, F. Trier, T. Wijnands, R. J. Green, N. Gauquelin, R. Egoavil, D. V. Christensen, G. Koster, M. Huijben, N. Bovet, S. Macke, F. He, R. Sutarto, N. H. Andersen, J. A. Sulpizio, M. Honig, G. E. D. K. Prawiroatmodjo, T. S. Jespersen, S. Linderoth, S. Ilani, J. Verbeeck, G. Van Tendeloo, G. Rijnders, G. A. Sawatzky, and N. Pryds, Nat. Mater. **14**, 801 (2015).

[14] P. E. Blöchl, Phys. Rev. *B* **50**, 17953 (1994).

[15] G. Kresse and D. Joubert, Phys. Rev. B **59**, 1758 (1999).

[16] G. Kresse and J. Furthmuller, Phys. Rev. B **54**, 11169 (1996).

[17] G. Louie, S. Froyen, and M. L. Cohen, Phys. Rev. B 26, 1738 (1982).

[18] H. M. Christen, G. E. Jellison Jr., I. Ohkubo, S. Huang, M. E. Reeves, E. Cicerrella, J. L. Freeouf, Y. Jia, and D. G. Schlom, Appl. Phys. Lett. **88**, 262906 (2006).

[19] H. J. Kim, J. Kim, T. H. Kim, W.-J. Lee, B.-G. Jeon, J.-Y. Park, W. S. Choi, D. W. Jeong, S. H. Lee, J. Yu, T. W. Noh, and K. H. Kim, Phys. Rev. B **88**, 125204 (2013).

[20] H. Mizoguchi, H. W. Eng, and P. M. Woodward, Inorg. Chem. **43**, 1667 (2004).

[21] H. J. Kim, J. Kim, T. H. Kim, W.-J. Lee, B.-G. Jeon, J.-Y. Park, W. S. Choi, D. W. Jeong, S. H. Lee, J. Yu, T. W. Noh, and K. H. Kim, Phys. Rev. B **88**, 125204 (2013).

[22] S. A. Chambers, T. C. Kaspar, A. Prakash, G. Haugstad, and B. Jalan, Appl. Phys. Lett. **108**, 152104 (2016).

[23] B. Li, Q. Liu, Y. Zhang, Z. Liu, and L. Geng, J. Alloys Comp. **680**, 343 (2016).

[24] V. V. Afanas'ev, A. Stesmans, L. F. Edge, D. G. Schlom T. Heeg, J. Schubert, Appl. Phys. Lett. **88**, 032104 (2006); Appl. Phys. Lett. **85**, 5917 (2004).

[25] R. Liferovich and R Mitchell, J. Sol. State Chem. **177**, 2188 (2004).

[26] T. Heeg, M. Wagner, J. Schubert, Ch. Buchal, M. Boese, M. Luysberg, E. Cicerrella, and J. L. Freeouf, Microelectr. Eng. **80**, 150 (2005).

[27] E. Cicerrella, J. L. Freeouf, L. F. Edge, D. G. Schlom, T. Heeg, J. Schubert, and S. A. Chambers, J. Vac. Sci. Tech. A **23**, 1676 (2005).

[28] H. J. Kim, U. Kim, H. M. Kim, T. H. Kim, H. S. Mun, B.-G. Jeon, K. T. Hong, W.-J. Lee, C. Ju, K. H. Kim, and K. Char, Appl. Phys. Exp. **5**, 061102 (2012); Phys. Rev. B **86**, 165205 (2012).

[29] D. O. Scanlon, Phys. Rev. B **87**, 161201 (2013).

[30] U. Kim, C. Park, T. Ha, Y. M. Kim, N. Kim, C. Ju, J. Park, J. Yu, J. H. Kim, and K. Char, APL Mater. **3**, 036101 (2015).

[31] S. Raghavan, T. Schumann, H. Kim, J. Y. Zhang, T. A. Cain, and S. Stemmer, APL Mater. **4**, 016106 (2016).

[32] S. Kobayashi, Y. Mizumukai, T. Ohnishi, N. Shibata, Y. Ikuhara, and T. Yamamot, ACS Nano **9**, 10769 (2015).

[33] J. Neugebauer and M. Scheffler, Phys. Rev. B **46**, 16067 (1992).

[34] X. Gonze, Phys. Rev. B **55**, 10337 (1997); X. Gonze and C. Lee, Phys. Rev. B **55**, 10355 (1997).

[35] S. Baroni, S. de Gironcoli, A. Dal Corso, and P. Giannozzi, Rev. Mod. Phys. **73**, 515 (2001).

[36] C. Zhao, T. Witters, B. Brijs, H. Bender, O. Richard, M. Caymax, T. Heeg, J. Schubert, V. V. Afanas'ev, A. Stesmans, and D. G. Schlom, Appl. Phys. Lett. **86**, 132903 (2005).

[37] W. Son, E. Cho, B. Lee, J. Lee, and S. Han, Phys. Rev. B **79**, 245411 (2009).

[38] S. Ryu, H. Zhou, T. R. Paudel, C. W. Bark, J. Irwin, J. Podkaminer, D. Lee, T. H. Kim, D. D. Fong, E. Y. Tsymbal, M. S. Rzchowski, and C. B. Eom, Appl. Phys. Lett. **111**, 141604 (2017).

[39] K. Krishnaswamy, B. Himmetoglu, Y. Kang, A. Janotti, and C. G. Van de Walle, Phys Rev B. 95, 205202 (2017)

[40] R. Pentcheva, M. Huijben, K. Otte, W. E. Pickett, J. E. Kleibeuker, J. Huijben, H. Boschker, D. Kockmann, W. Siemons, G. Koster, and H. J. Zandvliet, Phys. Rev. Lett. **104**, 166804 (2010).

[41] J. Lee and A. A. Demkov, Phys. Rev. B **78**, 193104 (2008).

[42] P. Delugas, A. Filippetti, V. Fiorentini, D. I. Bilc, D. Fontaine, and P. Ghosez, Phys. Rev. Lett. **160**, 166807 (2011).

[43] B. Himmetoglu, A. Janotti, H. Peelaers, A. Alkauskas, and C. G. Van de Walle, Phys. Rev. B **90**, 241204(R) (2014).

[44] A. Prakash, P. Xu, A. Faghaninia, S. Shukla, J. W. Ager III, C. S. Lo, and B. Jalan, Nat. Comm. **8**, 15167 (2017).

[45] J. Son, P. Moetakef, B. Jalan, O. Bierwagen, N. J. Wright, R. Engel-Herbert, and S. Stemmer, Nat. Mater. **9**, 482 (2010).

[46] S. Kobayashi, Y. Mizumukai, T. Ohnishi, N. Shibata, Y. Ikuhara, and T. Yamamot, ACS Nano **9**, 10769 (2015).

[47] A. Ohtomo, D. A. Muller, J. L. Grazul, and H. Y. Hwang, Nature **419**, 378 (2002).

[48] H. W. Jang, D. A. Felker, C. W. Bark, Y. Wang, M. K. Niranjan, C. T. Nelson, Y. Zhang, D. Su, C. M. Folkman, S. H. Baek, S. Lee, K. Janicka, Y. Zhu, X. Q. Pan, D. D. Fong, E. Y. Tsymbal, M. S. Rzchowski, and C. B. Eom, Science **331**, 886 (2011).

[49] K. V. Reich, M. Schecter, and B. I. Shklovskii, Phys. Rev. B **90**, 241204(R) (2014).